OXFORD GENETICS

GENETICS, 2024, 227(4), iyae101
https://doi.org/10.1093/genetics/iyae101
Advance Access Publication Date: 14 June 2024
Investigation

Calcium influx rapidly establishes distinct spatial recruitments of Annexins to cell wounds

Mitsutoshi Nakamura, Susan M. Parkhurst *

Basic Sciences Division, Fred Hutchinson Cancer Center, Seattle, WA 98109, USA

*Corresponding author: Basic Sciences Division, Fred Hutchinson Cancer Center, 1100 Fairview Ave N., A1-187, Seattle, WA 98109, USA. Email: susanp@fredhutch.org

To survive daily damage, the formation of actomyosin ring at the wound edge is required to rapidly close cell wounds. Calcium influx is one of the start signals for these cell wound repair events. Here, we find that the rapid recruitment of all 3 *Drosophila* calcium-responding and phospholipid-binding Annexin proteins (AnxB9, AnxB10, and AnxB11) to distinct regions around the wound is regulated by the quantity of calcium influx rather than their binding to specific phospholipids. The distinct recruitment patterns of these Annexins regulate the subsequent recruitment of RhoGEF2 and RhoGEF3 through actin stabilization to form a robust actomyosin ring. Surprisingly, while the wound does not close in the absence of calcium influx, we find that reduced calcium influx can still initiate repair processes, albeit leading to severe repair phenotypes. Thus, our results suggest that, in addition to initiating repair events, the quantity of calcium influx is important for precise Annexin spatiotemporal protein recruitment to cell wounds and efficient wound repair.

Keywords: cell wound repair; *Drosophila*; Annexin; calcium dynamics

Introduction

When cells encounter physical stresses that result in cortex ruptures, they must rapidly deploy their repair pathway to preserve cell homeostasis. Influx of extracellular calcium through the cortex breach is one of the most upstream events and is thought to initiate the repair process by activating downstream molecules (Cheng *et al.* 2015; Cooper and McNeil 2015; Moe *et al.* 2015; Andrews and Corrotte 2018; Nakamura *et al.* 2018; Ebstrup *et al.* 2021). Previous studies have shown that calcium influx as detected by calcium indicators (i.e. GCaMP) is uniform at the wound site (Terasaki *et al.* 1997; Davenport *et al.* 2016; Nakamura *et al.* 2020). How this uniform calcium signal is translated into the dynamic, yet precise, spatiotemporal recruitment and activity of downstream molecules is unknown. Upon cortex injury, vesicles are recruited to the wound forming a temporary membrane plug that seals the damaged area, followed by the assembly of an actomyosin ring at the wound edge linking the cortical cytoskeleton to the plasma membrane, which subsequently translocate inward to pull the wound edges closed (Sonnemann and Bement 2011; Cooper and McNeil 2015; Nakamura *et al.* 2018; Hui *et al.* 2022). After the wound closes, the membrane plug is removed from the wound site, the actomyosin ring is disassembled, and the cortical cytoskeleton and plasma membrane are remodeled to return to their original composition, organization, and functional states.

Annexins (Anxs) are a highly conserved family of calcium-responding proteins that bind specific phospholipids in a calcium-dependent manner (Blackwood and Ernst 1990; Gerke *et al.* 2005; Lizarbe *et al.* 2013). Anxs are known to play roles in wound repair: AnxA1, AnxA2, AnxA4, AnxA5, AnxA6, and AnxA7 (out of 13 mammalian Anxs) are rapidly recruited (within seconds) to wounds and associate with the plasma membrane to regulate different aspects of cell wound repair in a context-dependent manner (Lennon *et al.* 2003; McNeil *et al.* 2006; Carmeille *et al.* 2016; Davenport *et al.* 2016; Koerdt and Gerke 2017; Nakamura *et al.* 2017; Pervin *et al.* 2018; Sønder *et al.* 2019; Bittel *et al.* 2020; Croissant *et al.* 2020; Vicic *et al.* 2022). In MCF7 cells, AnxA4 has been suggested to induce membrane curvature and AnxA6 to induce membrane folding, which are necessary to generate the constriction force needed to pull the wound edge inward to close the gap (Boye *et al.* 2017). AnxA5 has been shown to form a 2D self-assembled lattice structure at wounds to reseal the damaged plasma membrane in mouse perivascular cells (Bouter *et al.* 2011). AnxA1, AnxA2, AnxA5, and AnxA6 are recruited to muscle cell wounds where they assemble into a compact structure on the extracellular surface of a cell, called a tight repair cap, for efficient wound repair (Demonbreun *et al.* 2016). AnxA6 has been shown to form a similar tight repair cap for efficient membrane repair in neurons (Demonbreun *et al.* 2022). In addition to dynamic membrane regulation, AnxA1, AnxA2, and AnxA6 have also been shown to regulate actin dynamics through binding to and/or bundling F-actin (Glenney *et al.* 1987; Ikebuchi and Waisman 1990; Hosoya *et al.* 1992; Hayes *et al.* 2004). In particular, AnxA2 binds to F-actin and regulates Rho-mediated actin rearrangement during cell adhesion and cytokinesis, and regulates actin polymerization and bundling during exocytosis and endosome biogenesis (Babbin *et al.* 2007; Rescher *et al.* 2008; Morel *et al.* 2009; Benaud *et al.* 2015; Gabel *et al.* 2015; Benaud and Prigent 2016).

Received on 04 February 2024; accepted on 09 June 2024

Using the *Drosophila* cell wound repair model, we have previously shown that AnxB9 is rapidly recruited to the wound where it regulates actin stabilization, which is necessary for the recruitment of RhoGEF2 to wounds during the repair process (Nakamura *et al.* 2017). Here, we show that the other 2 *Drosophila* Anxs, AnxB10 and AnxB11, are also recruited to wounds, where they are both required for RhoGEF3 recruitment to wounds. Strikingly, all 3 Anxs are recruited to wounds within 3 s post-wounding, exhibit distinct but adjacent spatial recruitment patterns, and have non-redundant functions in actomyosin ring formation during cell wound repair. Interestingly, while Anxs are not recruited to wounds in the absence of a calcium influx, we find that reduced calcium influx alters their recruitment patterns. Thus, our results indicate that calcium influx upon wounding not only triggers the repair process but creates distinct spatiotemporal protein recruitment patterns of molecules such as the Anxs.

Materials and methods

Reagents used in this study are described in Supplementary Table 1

Fly stocks and genetics

Flies were cultured and crossed at 25°C on yeast–cornmeal–molasses–malt medium. Flies used in this study are described in Supplementary Table 1. All fly stocks were treated with tetracycline and then tested by PCR to ensure that they did not harbor Wolbachia.

To knockdown genes, RNAi lines were driven maternally using the GAL4-UAS system (Brand and Perrimon 1993) with P{matalpha4-GAL-VP16}V37 and used 2 independent RNAi lines each for AnxB10 and AnxB11 (Supplementary Table 1). vermillion RNAi was used for control. Localization patterns and mutant analyses were performed at least twice from independent genetic crosses, and ≥10 embryos were examined unless otherwise noted. Images representing the average phenotype were selected for figures. We used FlyBase (release FB2024_03) to find information on phenotypes/function/stocks/gene expression/sequences (etc) (Öztürk-Çolak *et al.* 2024).

Generation of fluorescently tagged Annexins and lipid biosensors

RNAi lines for AnxB11 were generated using the method previously described (Ni *et al.* 2011). 2 oligos were annealed and cloned into pWALIUM22 (DGRC_1473). pWALIUM22-AnxB11 RNAi(1) and RNAi(2) were injected into M{3xP3-RFP.attP}ZH-86Fb (BDSC_24749).

To generate the StFP knock-in AnxB10, we used CRIMIC technology (Lee *et al.* 2018). We replaced the GAL4 cassette in AnxB10[CR00582-TG4.0] allele with StFP.

To generate sqh-sfGFP-AnxB10, the AnxB10 ORF was amplified from BDGP clone LD25605 and fused 5′ to sfGFP. The resulting sfGFP-AnxB10 fusion was cloned into pSqh5′+3′UTR (MT) as a 5′ StuI-3′ XbaI fragment.

To generate AnxB11-StFP, a genomic region of AnxB11, including 5 kb upstream from the start codon and 2.2 kb downstream from the stop codon, was amplified and cloned into pCasper4 with StFP inserted just before the AnxB11 start codon.

To generate Ubi-StFP-8PM, StFP-8PM was amplified by adding prenylated octavalent peptides (+8pre: ARDGRRRRRRARARCVIM; Eisenberg *et al.* 2021) to C-terminus of StFP. StFP-8PM was cloned into pUbi5′+3′UTR as a 5′ StuI-3′ XbaI fragment. StFP-8PM binds to plasma membrane electrostatic properties dependently and gives a cleaner label than general membrane reporters/dyes such as FM-4-64.

To generate the phosphatidylserine (PS) biosensor, Lact-C2 was amplified from Lact-C2-GFP (Addgene #22852) and fused 5′ to StFP. The resulting Lact-C2-StFP fusion was cloned into UASz as a 5′ KpnI and 3′ XbaI fragment. Lact-C2-StFP localizes in the plasma membrane as previously described [Supplementary Fig. 1; (Yeung *et al.* 2008)].

To generate the phosphatidic acid (PA) biosensor, the PASS sequence was amplified from a GFP-PASS plasmid [provided by G. Du, University of Texas Health Science Center at Houston, Houston, Texas; (Zhang *et al.* 2014)] and fused 5′ to sfGFP. The resulting sfGFP-PASS fusion was cloned into UASz as a 5′ KpnI and 3′ XbaI fragment. sfGFP-PASS localizes in the plasma membrane as previously described [Supplementary Fig. 1; (Thakur *et al.* 2019)].

To generate transgenic flies, each construct (500 µg/ml) was injected along with the pTURBO helper plasmid (100 µg/ml) into isogenic w1118 flies as previously described (Spradling 1986). Lact-C2-StFP and GFP-PASS constructs were injected into M{3xP3-RFP.attP}ZH-86Fb (BDSC_24749).

Embryo handling and preparation

Nuclear cycle (NC) 4–6 *Drosophila* embryos were collected from 0 to 30 min at room temperature (22°C). Embryos were hand dechorionated, placed onto No. 1.5 coverslips coated with glue, and covered with Series 700 halocarbon oil (Halocarbon Products Corp).

Laser wounding

All wounds were generated with a pulsed nitrogen N2 Micropoint laser (Andor Technology Ltd., Concord, MA, USA) tuned to 435 nm and focused on the cortical surface of the embryo. A region of interest was selected in the lateral midsection of the embryo, and ablation was controlled by MetaMorph. On average, ablation time was less than 3 s, and time-lapse imaging was initiated immediately. Occasionally, a faint grid pattern of fluorescent dots is visible at the center of wounds that arise from damage to the vitelline membrane that covers embryos.

Drug injections

Pharmacological inhibitors were injected into NC4–6 staged *Drosophila* embryos, incubated at room temperature (22°C) for 5 min, and then subjected to laser wounding. The following inhibitors were used: phalloidin (100 µg/ml; Thermo Fisher Scientific), BAPTA (100 mM or 50 mM; Invitrogen), and EGTA (100 mM; Sigma-Aldrich). Phalloidin was prepared in an injection buffer (5 mM KCl, 0.1 mM NaP, pH 6.8). BAPTA and EGTA were prepared in water.

Immunostaining of ovaries

Female flies were fattened on yeast for 2 days, and then, ovaries were dissected into cold PBS. Ovaries were fixed using 1:6 fix/heptane for 10 min. Fix is: 16.7 mM KPO4 pH 6.8, 75 mM KCl, 25 mM NaCl, 3.3 mM MgCl2, and 6% formaldehyde. After 3 washes with PBS plus 0.1% Triton X-100, ovaries were permeabilized in PBS plus 1% Triton X-100 at room temperature for 2 h. Ovaries were washed 3 times with PAT [1× PBS, 0.1% Tween-20, 1% bovine serum albumin (BSA), 0.05% azide] and then blocked in PAT at 4°C for 2 h. Antibodies were used at the following concentrations: rabbit anti-GFP monoclonal (1:2000; Invitrogen), and mouse anti-Hrs (1:40; Developmental Study Hybridoma Bank), and the ovaries incubated overnight at 4°C. Ovaries were washed 3 times with Normal Serum Wash (1× PBS, 0.1% Tween-20, 0.1% BSA, 4% normal goat serum) for 40 min each, then incubated with Alexa Fluor 488-conjugated secondary antibodies, Alexa Fluor 568-conjugated secondary antibodies, and Alexa Fluor

633-conjugated secondary antibodies (1:1,000; Invitrogen) overnight at 4°C. Ovaries were washed with PTW (1× PBS, 0.1% Tween- 20), incubated with Alexa Fluor 568-conjugated Phalloidin at 0.005 units/µl (Molecular Probes/Invitrogen, Rockford, IL) at room temperature for 1 h, and then washed with PTW. Ovaries were dissected into individual ovarioles and then mounted on slides in Slowfade Gold (Invitrogen). A minimum of 2 biological replicates were performed for each condition.

Microscopy

All imaging was performed at room temperature (22°C). The following microscope was used: For live imaging, Revolution WD systems (Andor Technology Ltd., Concord, MA, USA) mounted on a Leica DMi8 (Leica Microsystems Inc., Buffalo Grove, IL, USA) with a 63×/1.4 NA objective lens and controlled by MetaMorph software. Images and videos were acquired with 488 and 561 nm, using an Andor iXon Ultra 897 or 888 Electron Multiplying Charge-Coupled Device cameras (Andor Technology Ltd., Concord, MA, USA). All images for cell wound repair were 12–20 µm stacks/0.25 µm steps. To examine each Anx recruitment to the wound without other reporters, images were acquired every 5 s. To examine Anx recruitment relative to actin and other Anxs, images were acquired every 15 s with dual camera mode using 2 Andor iXon 888. To examine calcium dynamics using GCaMP6s, images were acquired every 15 s. To examine RNAi knockdown phenotypes, images were acquired every 30 s for 15 min and then every 60 s for 25 min. To examine RhoGEF recruitment to the wound, images were acquired every 45 s. Imaging parameters were determined based on brightness, photobleaching, and duration of time-lapse.

For fixed ovaries, Zeiss LSM 780 spectral confocal microscope (Carl Zeiss Microscopy GmbH, Jena, Germany) fitted with Zeiss Plan-Apochromat 40×/1.4 oil Plan-Apochromat objectives. FITC (Alexa 488) fluorescence was excited with the 488-nm line of an Argon laser, and detection was between 498 and 560 nm. Red (Alexa 568) fluorescence was excited with the 561-nm line of a diode-pumped solid-state laser, and detection was between 570 and 670 nm. Far-red (Alexa 633) fluorescence was excited with the 633 line of an Argon laser, and detection was between 570 and 670 nm. Pinhole was typically set to 1.0 Airy Units. Confocal sections were acquired at 0.25–1.0 micron spacing.

Image processing, analysis, and quantification

All images were analyzed with Fiji (Schindelin *et al.* 2012) and Matlab (Mathworks). Measurements of the wound area were done manually. To generate xy kymographs, all time-lapse xy images were cropped to 5.5 µm × 98.1 µm, and then, each cropped image was lined up. For fluorescent line plots, the mean fluorescence profile intensities were calculated from 51 equally spaced radial profiles anchored at the center of the wound, swept from 0° to 180° (Hui *et al.* 2023). Radial profiles of diameter 301 pixels were used. To normalize the signal intensity in ≥10 embryos, the intensity in each pixel was divided by the max intensity in each embryo. The lines represent the averaged fluorescent intensity from ≥10 embryos, and the gray area is the 95% confidence interval.

Quantification of the width and average intensity of actin ring, wound expansion, and closure rate was performed as follows: the width of the actin ring was calculated with 2 measurements, the ferret diameters of the outer and inner edge of the actin ring at 120 s post-wounding. Using these measurements, the width of the actin ring was calculated with (outer feret diameter−inner feret dimeter)/2. The average intensity of the actin ring was calculated with 2 measurements. Instead of measuring ferret diameters, we measured area and integrated intensity in the same regions as described in ring width. Using these measurements, the average intensity in the actin ring was calculated with (outer integrated intensity−inner integrated intensity)/(outer area−inner area). To calculate the relative intensity for unwounded (UW) time point, the average intensity at UW was measured with 50 × 50 pixels at the center of embryos, and then, the averaged intensity of the actin ring at each timepoint was divided by the average intensity of UW. Wound expansion was calculated with max wound area/initial wound size. Closure rate was calculated with 2 time points, one is t_{max} that is the time of reaching maximum wound area, and the other is $t <$ half that is the time of reaching 50–35% size of max wound since the slope of wound area curve changes after $t <$ half. Using these time points, the average speed was calculated with (wound area at t_{max}−wound area at $t <$ half)/t_{max}-$t <$ half. To quantify RhoGEF recruitment to wounds, we subtracted the fluorescent intensity of the pre-wounding time point from the 135 s post-wounding image. We then measured the averaged fluorescent intensity from radial line plots (described above) in the subtracted image. Line profiles were plotted, and the area under the curve (AUC) was measured (Nakamura *et al.* 2017). Generation of all graphs and a one-way ANOVA test were performed with Prism 8 (GraphPad Software Inc.) or Matlab (Mathworks).

Protein expression

AnxB9, AnxB10, and AnxB11 cDNAs were amplified as 5′ BamHI-3′ NotI fragments from cDNA clones (DGRC). 2xFYVE was amplified as 5′ BamHI-3′ NotI fragments from genomic DNA of UAS-GFP-myc-2xFYVE; Lact-C2 and PABD was amplified as 5′ BamHI-3′ NotI fragments from Lact-C2-GFP and GFP-PASS plasmids described above, respectively. All fragments were cloned into a double tag pGEX-dt vector [GST and His; (Liu *et al.* 2009)] with FLAG tag at the N-terminus of protein. For Anx and 2xFYVE protein purification, cells were lysed by sonication in lysis buffer (50 mM Tris pH 7.6, 100 mM NaCl, 1 mM EGTA, 5% Glycerol, and 1 mM DTT) with 1% Triton X, 50 mM imidazole, and Complete protease inhibitor tablets (ThermoFisher). Lysates were centrifuged at 10,000g for 30 min and the supernatants were coupled to Fastflow nickel-sepharose (GE) for 3 h at 4°C. The matrix was washed 3 times with lysis buffer with 50 mM imidazole and eluted by lysis buffer with 1 M imidazole. All His elutions were coupled to glutathione-sepharose 4B (GE) for 3 h at 4°C, washed with lysis buffer, and then eluted with Human Rhinovirus 3C protease (ThermoFisher). Eluted proteins were dialyzed into storage buffer (50 mM Tris pH 7.6, 100 mM NaCl, 5% Glycerol, 1 mM DTT) and then flash frozen. For protein Lact-C2, and PABD purification, PBS was used instead of Tris.

Lipid protein interaction assay

PIP strip membranes (Invitrogen) were blocked in blocking buffer (TBS: 20 mM Tris pH 8.0 + 150 mM NaCl, with 0.1% Tween-20 and 1% non-fat milk) for 1 h at RT and incubated with purified Anx proteins (0.5 µg/ml) and 100 µM $CaCl_2$ or 100 µM EGTA for 1 h at RT. The membranes were washed 3 times with TBS-T (TBS with 0.1% Tween-20), and bound Anxs were detected by immunoblotting using Rat anti-FLAG antibody (1:5000; Biolegend) and ECL (ThermoFisher). 2xFYVE, Lact-C2, and PABD proteins were used as positive controls for PI3P, PS, and PA (Supplementary Fig. 1). PBS was used instead of Tris for Lact-C2 and PABD proteins.

qPCR

Total RNA was obtained from 100 embryos (0–30 min old) using TRIzol (Invitrogen). 1 µg of total RNA was used for reverse

transcription with the iScript gDNA Clear cDNA Synthesis Kit (Bio-Rad). RT-PCR analysis was performed using the iTaq Universal SYBR Green Supermix (Bio-Rad) with 2 individual parent sets and 2 technical replicates on the CFX96TM Real Time PCR Detection System (Bio-Rad). RpL32 was used as a reference gene. The % knockdown was calculated using the ΔΔCq calculation method compared with control (vermilion knockdown). Same primer sets RpL32 were used in the previously described (Nakamura *et al.* 2020).

Statistical analysis

All statistical analysis was done using Prism 8 (GraphPad, San Diego, CA). Gene knockdowns were compared to the appropriate control, and statistical significance was calculated using a one-way ANOVA test or Welch's *t*-test with $P < 0.05$ considered significant.

Results

All 3 *Drosophila* Annexins are rapidly recruited to wounds and exhibit distinct spatial recruitment patterns

We previously showed that the rapid spatial and temporal recruitment of RhoGEF2 to wounds is regulated by AnxB9 (Fig. 1a and b) (Nakamura *et al.* 2017). Since RhoGEF3 and Pbl are still recruited to wounds in the AnxB9 knockdown background, we investigated if the other 2 *Drosophila* Anxs—AnxB10 and AnxB11—regulate the spatial and/or temporal recruitment of these two RhoGEFs during cell wound repair. If so, both AnxB10 and AnxB11 would be expected to be recruited to wounds before RhoGEF patterns are established (<15 s post-wounding). To examine the response of AnxB10 and AnxB11 during cell wound repair, we generated 3 fly transgenic lines expressing: (1) sfGFP-AnxB10 driven by the Myosin regulatory light chain [Spaghetti Squash (Sqh)] promoter, (2) mScarlet (StFP)-AnxB10 (knock-in), and (3) StFP-AnxB11 under the control of the endogenous AnxB11 promoter. We examined embryos co-expressing these fluorescently tagged Anxs and an actin reporter (sGMCA or sStMCA; see *Methods*). Wounds were generated by laser ablation on the lateral side of nuclear cycle 4–6 *Drosophila* embryos (see *Methods*). In this cell wound repair model, actin accumulates in 2 adjacent regions: (1) a highly enriched ring at the wound edge, and (2) a less dense halo region encircling the actomyosin ring at the wound edge (Fig. 1a; Abreu-Blanco *et al.* 2011).

Upon wounding, both AnxB10 and AnxB11 are rapidly recruited to wounds (<3 s), similar to that observed with AnxB9 (Fig. 1b–d; Nakamura *et al.* 2017). While their temporal recruitment is similar, the 3 Anx spatial recruitments to wounds differ. AnxB9 recruitment forms 2 distinct ring-like structures: a thin discontinuous ring with punctate accumulation inside the actin ring and a wide diffuse outer ring whose inner edge overlaps with the actin ring (Fig. 1b and e–e'). AnxB10 is recruited in a sharp ring that is inside and juxtaposed to the actin ring (Fig. 1c and f–f'). AnxB11 is recruited in a robust ring that overlaps with the actin ring and is also recruited to the area inside of the actin ring in a diffuse distribution (Fig. 1d and g–g'). These distinct Anx spatial recruitment patterns were confirmed when examining different combinations of fluorescently tagged Anxs (Fig. 1h–j'). Overall, the 3 Anxs exhibit distinct spatial recruitment patterns compared to each other (Fig. 1k), but which are similar to those observed for the 3 RhoGEFs that they regulate (Nakamura *et al.* 2017).

Drosophila Annexins have non-redundant functions in cell wound repair

The distinct spatial recruitment patterns of Anxs to wounds suggest that each Anx has a different role during cell wound repair. To investigate this, we examined wound repair dynamics of embryos expressing an actin reporter [sGMCA; (Kiehart *et al.* 2000)] in each Anx RNAi knockdown background (Figs. 2 and 3). As previously described, AnxB9 knockdown embryos exhibit wound overexpansion, slow wound repair, decreased actin ring width, and lower actin accumulation in the actin ring [Figs. 2a–b' and i, 3e–h; Supplementary Table 2; Supplementary Video 1 (Nakamura *et al.* 2017)]. AnxB10 knockdown embryos also exhibit wound overexpansion, slow wound repair, decreased actin ring width, and lower actin accumulation in the actin ring (Figs. 2c–e' and j, l; 3e–h; Supplementary Table 2; Supplementary Video 1). While AnxB11 knockdown and knockout embryos exhibit wound overexpansion and lower actin accumulation in the actin ring, contraction rates, and actin ring width are similar to control embryos (Fig. 2f–h', k and l, Fig. 3e–h; Supplementary Table 2; Supplementary Video 1). Thus, the recruitment patterns of Anxs to wounds and their knockdown phenotypes indicate that each Anx acts non-redundantly in regulating actin ring dynamics during cell wound repair.

Since a previous study in mammalian tissue culture cells suggested that Anxs constrict the plasma membrane breach through binding directly to the plasma membrane during cell wound repair (Davenport *et al.* 2016; Boye *et al.* 2017), we next examined whether *Drosophila* Anxs could close plasma membrane wounds independently of actin ring closure. To visualize the plasma membrane in our system, we wounded embryos co-expressing a plasma membrane reporter (Ubi-StFP-8PM), along with an actin reporter, in a triple Anx knockdown (AnxB9 RNAi + AnxB10 RNAi + AnxB11 RNAi) background. We find that closure of both the actin ring and plasma membrane breaches are still highly correlated in the triple Anx knockdown background, with these triple knockdown embryos exhibiting wound overexpansion, slow wound repair, decreased actin ring width, and lower actin accumulation in the actin ring (Fig. 3a–h; Supplementary Table 2; Supplementary Video 1). Hence, in the context of *Drosophila* cell wound repair, it is unlikely that Anxs regulate membrane dynamics actin independently to close wounds.

AnxB10 and AnxB11 regulate RhoGEF2 and RhoGEF3 recruitment to cell wounds

Since AnxB10 and AnxB11 are recruited to wounds earlier than RhoGEFs, have similar spatial recruitment patterns to wounds as RhoGEFs, and have non-redundant functions for actin ring dynamics during cell wound repair, we expected that AnxB10 and AnxB11 would regulate RhoGEF3 and Pbl recruitment to wounds, respectively. We wounded embryos co-expressing sfGFP-RhoGEF3 or Pbl-eGFP, along with an actin reporter, in AnxB10 or AnxB11 knockdown backgrounds (Fig. 4a–h). In control embryos, RhoGEF3 is recruited to the actin ring and outside the ring, and Pbl is recruited outside the actin ring (Fig. 4a and f). Surprisingly, Pbl is still recruited to wounds in both AnxB10 and AnxB11 knockdown backgrounds, indicating that its regulation does not depend on Anxs. In contrast, RhoGEF3 is no longer recruited to wounds in either of the AnxB10 and AnxB11 knockdown backgrounds (Fig. 4a–c, f–h, n and o). To determine if AnxB10 and AnxB11 regulate RhoGEF3 recruitment to the wound by stabilizing actin as AnxB9 does for RhoGEF2, we examined RhoGEF3 recruitment to the wound in embryos injected with phalloidin (actin stabilizer). Intriguingly, the recruitment of RhoGEF3 to the wound in AnxB10 and AnxB11 knockdown backgrounds is partially rescued by phalloidin injection, suggesting that both of these Anxs work upstream of RhoGEF3 through actin stabilization (Fig. 4d, e and n). Since RhoGEF2 recruitment to the wound also depends on actin stabilization, we wounded embryos co-expressing sfGFP-RhoGEF2

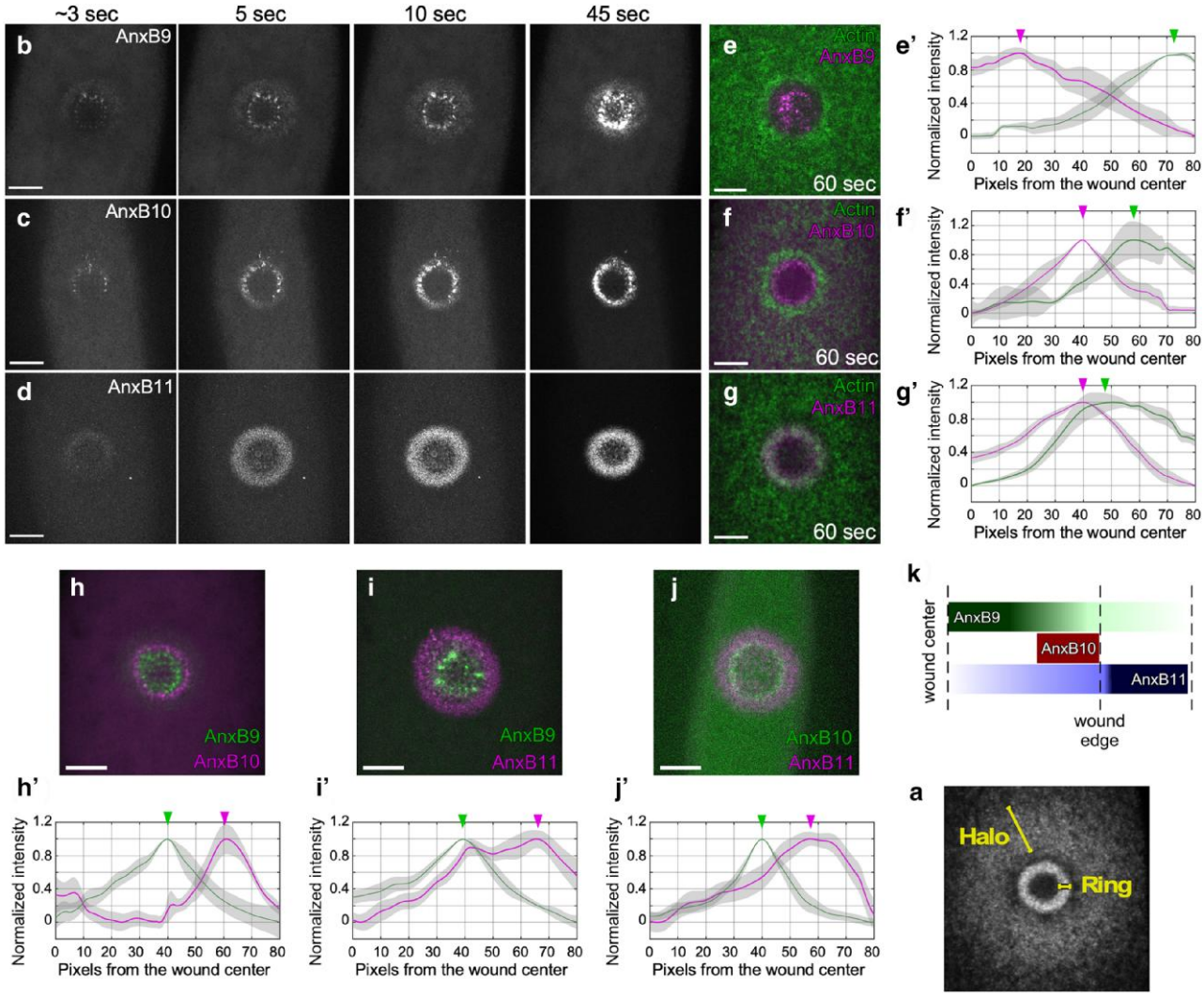

Fig. 1. The 3 *Drosophila* Anxs are rapidly recruited to distinct regions around the wound. a) Confocal xy projection image from a wounded NC4–6 *Drosophila* embryo expressing an actin reporter (sGMCA). (b–d) Confocal xy projection image from a wounded NC4–6 *Drosophila* embryo expressing GFP-AnxB9 (b), sfGFP-AnxB10 (c), or StFP-AnxB11 (d). (e–g) Confocal xy projection image from a wounded NC4–6 *Drosophila* embryo expressing an actin reporter (sGMCA or sStMCA) and GFP-AnxB9 (e), StFP-AnxB10 (f), or StFP-AnxB11 (g). (e'–g') Normalized fluorescence intensity profile at 60 s post-wounding from ≥10 embryos expressing sStMCA/GFP-AnxB9 (e'; $n = 13$), sGMCA/AnxB10 (f'; $n = 10$), and sGMCA/StFP-AnxB11 (g'; $n = 10$). Fluorescence peaks are indicated by arrowheads. (h–j) Confocal xy projection image from a wounded NC4–6 *Drosophila* embryo expressing GFP-AnxB9/StFP-AnxB10 (h), GFP-AnxB9/StFP-AnxB11 (i), and sfGFP-AnxB10/StFP-AnxB11 (j). (h'–j') Normalized fluorescence intensity profile at 60 s post-wounding from ≥10 embryos expressing GFP-AnxB9/StFP-AnxB10 (h'; $n = 10$), GFP-AnxB9/StFP-AnxB11 (i'; $n = 11$), and sfGFP-AnxB10/StFP-AnxB11 (j'; $n = 13$). (k) Schematic diagram summarizing the localization patterns of 3 Anxs at the wound edge. Scale bar: 20 µm. Time after wounding is indicated. In fluorescence intensity profiles, the line represents the averaged fluorescent intensity, and the gray area is the 95% confidence interval. Fluorescence peaks are indicated by arrowheads.

and the actin reporter in AnxB10 and AnxB11 RNAi backgrounds. As expected, RhoGEF2 is no longer recruited to the wound in AnxB10 and AnxB11 RNAi backgrounds (Fig. 4i–k and p). Surprisingly, in this context, RhoGEF2 recruitment is not rescued by actin stabilization (phalloidin injection; Fig. 4l, m and p). Thus, AnxB10 and AnxB11 must regulate another aspect of actin dynamics in addition to actin stabilization during cell wound repair. Taken together, our results indicate that the 3 Anxs regulate spatial recruitment of RhoGEF2 and RhoGEF3 to wounds during cell wound repair through controlling actin dynamics.

Anx recruitment patterns to wounds are regulated by calcium dynamics rather than phospholipid membrane patterning

We next investigated how the rapid spatial recruitment patterns of Anxs to wounds are organized. Since Anxs are calcium-responding and phospholipid-binding proteins (Blackwood and Ernst 1990; Gerke *et al.* 2005; Lizarbe *et al.* 2013), we examined the possibilities that their specific recruitment patterns were in response to specific phospholipid patterns around the wound or in direct response to calcium dynamics at the wound. Previous studies showed that phospholipids such as PI(4,5)P2, PI(3,4,5)P3, PS, and PA in the plasma membrane are reorganized upon wounding in the tissue culture cell, *Xenopus* oocyte, and *Drosophila* cell wound models (Vaughan *et al.* 2014; Nakamura *et al.* 2020; Ashraf and Gerke 2021). We first examined the specificity of the 3 *Drosophila* Anxs for binding phospholipids using membrane lipid strips and purified FLAG-tagged Anx proteins. In the absence of calcium, none of the Anxs bind to any of the phospholipids (Fig. 5a and b). In the presence of calcium, all Anxs bind to PE and PS, albeit with different preferences: AnxB9 binds equally to PE and PS, AnxB10 binds preferentially to PE, and AnxB11 binds

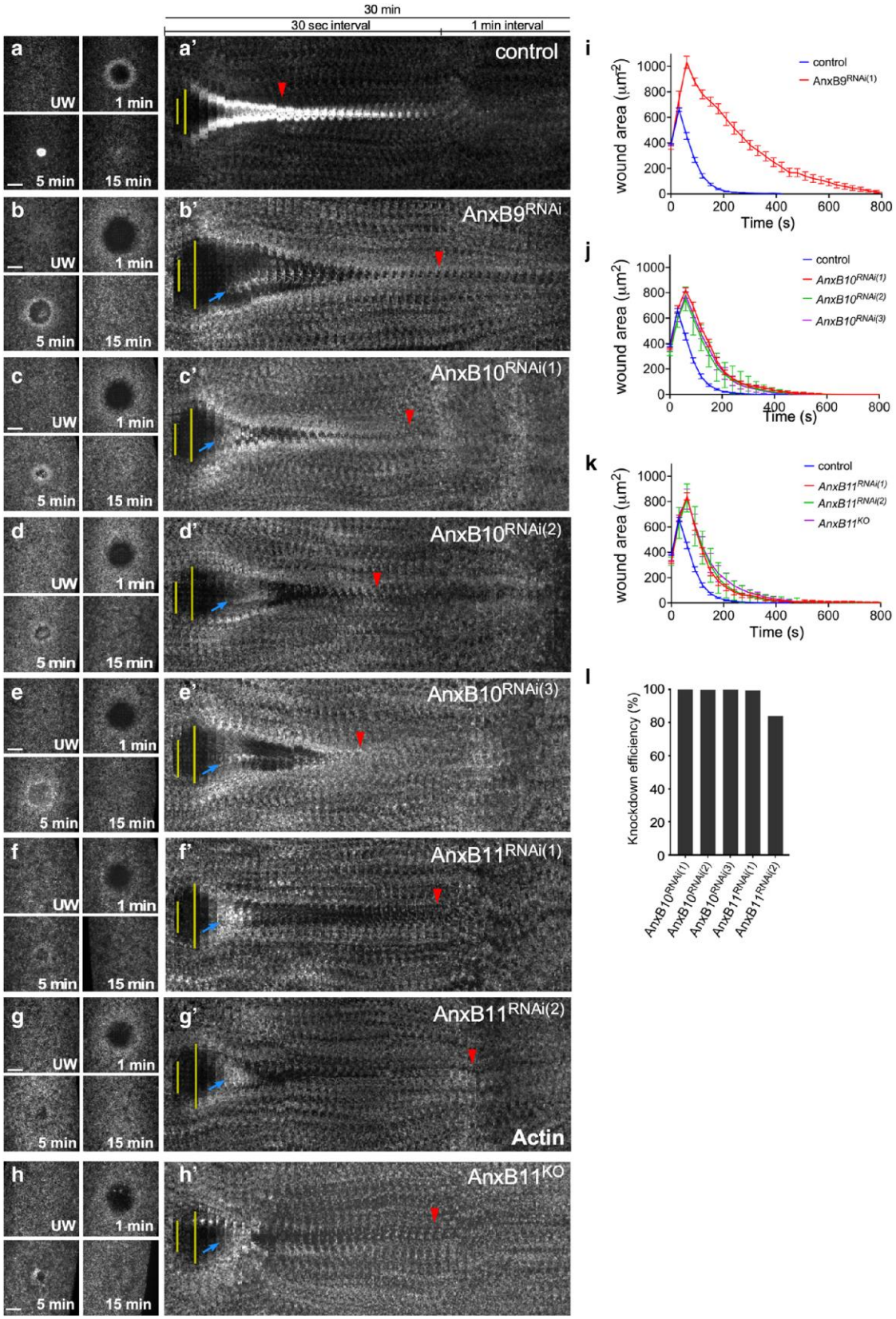

Fig. 2. The 3 Drosophila Anxs have non-redundant functions during cell wound repair. (a–h) Actin dynamics (sGMCA) during cell wound repair in NC4–6 staged *Drosophila* embryos: control (vermilion RNAi) (a), AnxB9 RNAi (b), AnxB10$^{RNAi(1)}$ (c), AnxB10$^{RNAi(2)}$ (d), AnxB10$^{RNAi(3)}$ (e), AnxB11$^{RNAi(1)}$ (f), AnxB11$^{RNAi(2)}$ (g), and AnxB11^{KO} (h). (a'–i') Kymographs across the wound area depicted in a–h, respectively. Wound expansion is highlighted by yellow lines. Actin accumulation internal to the wound is indicated by blue arrows. Completion of wound closure is indicated by red arrowheads. (i–k) Quantification of the wound area over time for control ($n = 14$), AnxB9 RNAi (i; $n = 10$), AnxB10$^{RNAi(1)}$ (j; $n = 10$), AnxB10$^{RNAi(2)}$ (j; $n = 10$), AnxB10$^{RNAi(3)}$ (j; $n = 10$), AnxB11$^{RNAi(1)}$ (k; $n = 10$), AnxB11$^{RNAi(2)}$ (k; $n = 10$), and AnxB11^{KO} (k; $n = 11$), (l) qPCR analysis of knockdown efficiency in AnxB10$^{RNAi(1)}$, AnxB10$^{RNAi(2)}$, AnxB10$^{RNAi(3)}$, AnxB11$^{RNAi(1)}$, and AnxB11$^{RNAi(2)}$ embryos under our imaging conditions. Error bars represent ± SEM. Scale bar: 20 μm. Time after wounding is indicated.

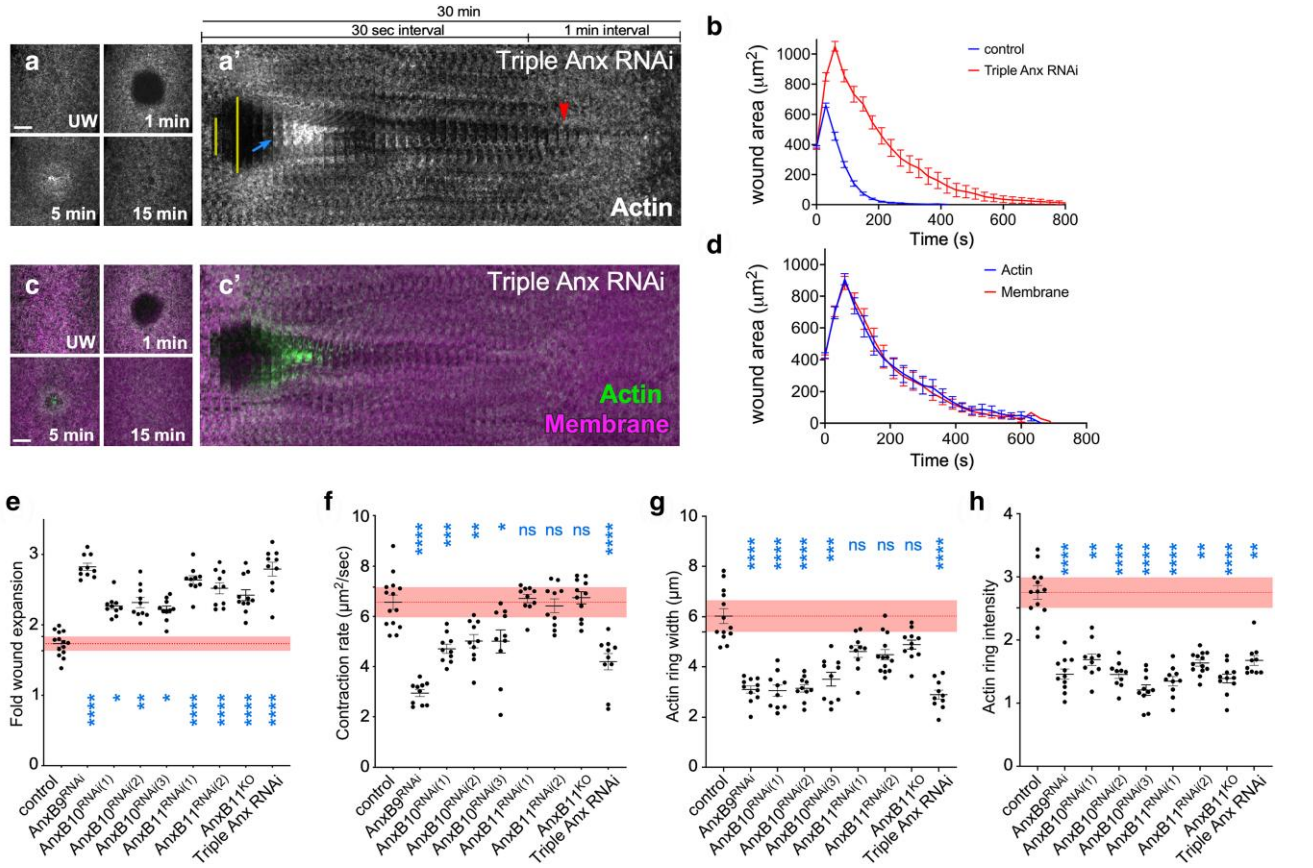

Fig. 3. The quantification of Anx knockdown phenotypes. (a, b) Actin and membrane dynamics (sGMCA and StFP-8PM, respectively) during cell wound repair in triple Anx knockdown embryos. (a'-b') Kymographs across the wound area depicted in a, b, respectively. (c, d) Quantification of the wound area over time measured from actin (sGMCA, c) and membrane (StFP-8PM, d) reporters in triple Anx knockdown embryos ($n = 10$). Scale bar: 20 μm. Time after wounding is indicated. (e–h) Quantification of fold wound expansion (e), contraction rate (f), actin ring width (g), and actin ring intensity (h) for control, AnxB9 RNAi, AnxB10 RNAi, AnxB11 RNAi, AnxB11^{KO}, and triple Anx RNAi. Error bars represent ± SEM. ANOVA tests were performed in e–h: $^{*}P < 0.05$, $^{**}P < 0.01$, $^{***}P < 0.001$, $^{****}P < 0.0001$, ns is not significant.

preferentially to PS (Fig. 5b). In addition to these in vitro assays, available phospholipid biosensors, including one for PS, do not mimic rapid Anx recruitment patterns around the wound (Fig. 5c–e', Supplementary Fig. 1; see *Methods*). Thus, Anxs recruitment patterns to wounds are unlikely created by simply responding to phospholipid patterns around wounds.

We next examined if calcium dynamics regulate Anx recruitment to wounds (Fig. 6). Extracellular calcium influx is thought to be an initial wound repair start signal in many cell wound repair models (Cooper and McNeil 2015; Moe *et al.* 2015; Andrews and Corrotte 2018; Nakamura *et al.* 2018; Ebstrup *et al.* 2021). *Drosophila* embryos are surrounded by an impermeable vitelline membrane (Fig. 6a). Similar to other models, extracellular fluid—in this case from the perivitelline space (extracellular space between the embryo and vitelline membrane)—is a major calcium source for calcium influx upon wounding in the *Drosophila* model (Nakamura *et al.* 2020). Injection of the calcium chelator BAPTA (100 mM) or EGTA (100 mM) into the perivitelline space of embryos expressing the calcium reporter GCaMP6 s removes almost all GCaMP signal around wounds (Nakamura *et al.* 2020; Fig. 6b–d). On the other hand, calcium influx was still observed in embryos expressing GCaMP6 s injected with half the concentration of BAPTA (50 mM) into perivitelline space, but GCaMP signals and diffusion were lower than those of the control (Fig. 6e–g). Using these 2 different concentrations of BAPTA injection (100 and 50 mM), we examined Anx recruitment patterns around the wound in different calcium influx backgrounds. In 100 mM BAPTA injection, none of the Anxs is recruited to wounds (Fig. 6h–n), which is consistent with previous studies using different models (Demonbreun *et al.* 2016; Koerdt and Gerke 2017; Bittel *et al.* 2020). Surprisingly, upon 50 mM BAPTA injection, all Anxs are recruited, but the recruitment patterns around the wounds are different from that of control buffer injections (Fig. 6o–q). AnxB9 exhibits an asymmetric and punctate ring-like pattern at the wound edge (Fig. 6n and o–o'). AnxB10 recruitment pattern is highly disrupted and exhibits a smaller number of puncta at the wound edge (Fig. 6n and p–p'). AnxB11 is recruited inside the wound in a punctate pattern (Fig. 6n and q–q'). Thus, rapid Anx spatial recruitment patterns upon wounding are influenced by the quantity of the calcium influx.

The quantity of the calcium influx is important for efficient cell wound repair

Since our results suggest that the quantity of calcium influx affects cell wound repair, we examined repair dynamics in embryos expressing an actin reporter that were injected with 100 mM or 50 mM BAPTA (Fig. 7; Supplementary Video 2). In 100 mM BAPTA injection, no actin ring forms around the wound site and the wound does not close, albeit oscillations in wound size due to embryonic development were observed (Fig. 7a–b', d and e; Supplementary Video 2). Thus, extracellular calcium is indispensable for repair in the *Drosophila* cell wound model. We expected that the wound in the absence of extracellular calcium would exhibit

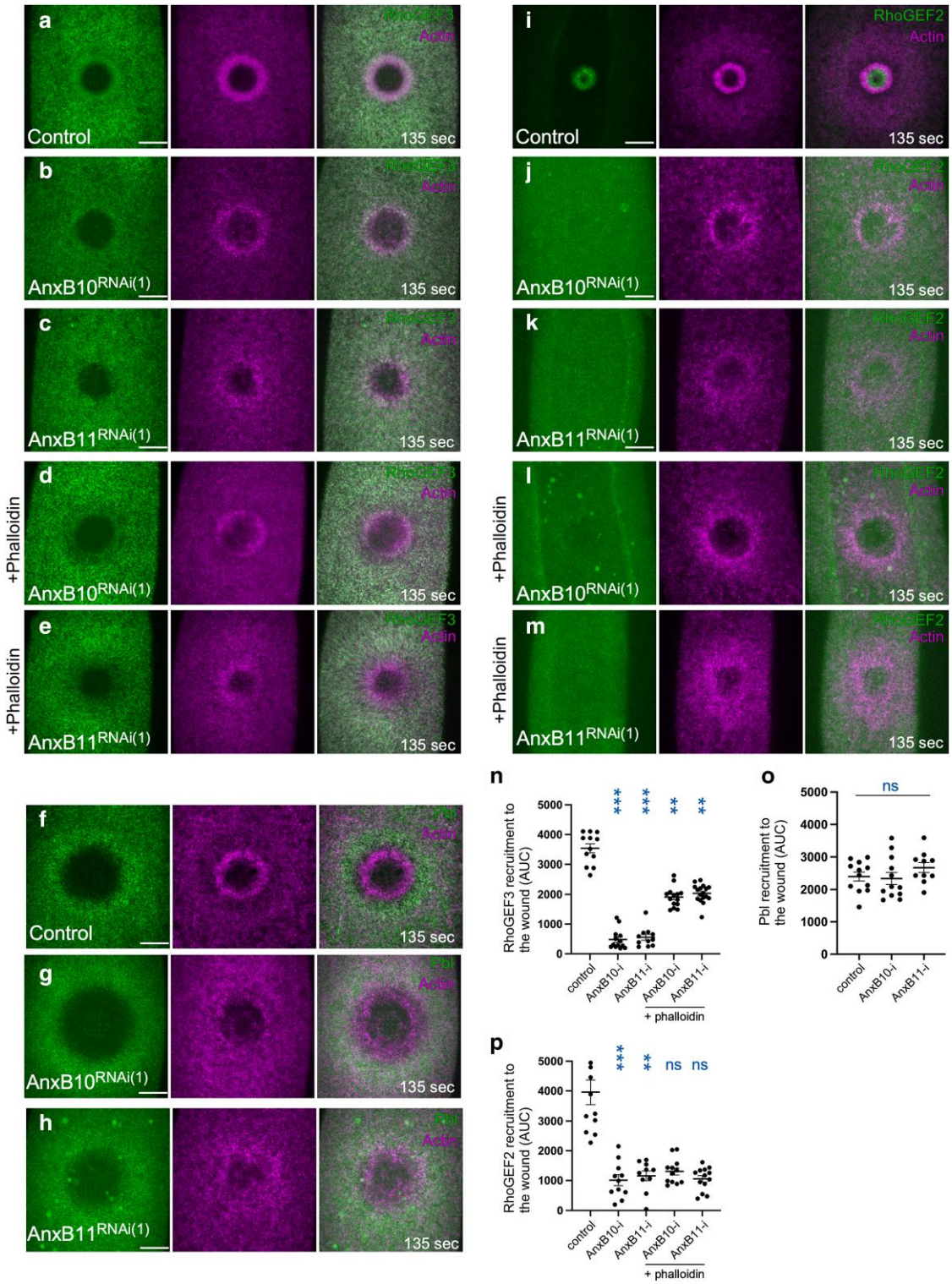

Fig. 4. AnxB10 and AnxB11 are required for RhoGEF2 and RhoGEF3 recruitment to the wound. (a–e) Localization of sfGFP-RhoGEF3 along with actin reporter (sStMCA) in control (a), AnxB10$^{RNAi(1)}$ (b), AnxB11$^{RNAi(1)}$ (c), AnxB10$^{RNAi(1)}$ + phalloidin (d), and AnxB11$^{RNAi(1)}$ + phalloidin (e) backgrounds. (f–h) Localization of Pbl-eGFP along with actin reporter (sStMCA) in control (f), AnxB10$^{RNAi(1)}$ (g), and AnxB11$^{RNAi(1)}$ (h) backgrounds. (i–m) Localization of sfGFP-RhoGEF3 along with actin reporter (sStMCA) in control (i), AnxB10$^{RNAi(1)}$ (j), AnxB11$^{RNAi(1)}$ (k), AnxB10$^{RNAi(1)}$ + phalloidin (l), and AnxB11$^{RNAi(1)}$ + phalloidin (m) backgrounds. (n–p) Quantification of the area under the curve in each fluorescence intensity profile from individual embryos for RhoGEF3 (n), Pbl (o), and RhoGEF2 (p). ns, not significant. ANOVA tests were performed in n–p. n and time after wounding are indicated. Scale bar: 20 μm. Error bars represent ± SEM.

overexpansion since wound expansion and actin ring formation are correlated (Abreu-Blanco *et al.* 2011), and Anx knockdowns exhibit overexpansion phenotypes (Fig. 3a). Interestingly, wound expansion was not significantly different between control and extracellular 100 mM BAPTA injected embryos (Fig. 7e). In 50 mM BAPTA injections, wounds exhibited the overexpansion phenotype, delayed initiation of wound closure, actin accumulation inside the wound, a disrupted actin ring, and longer wound

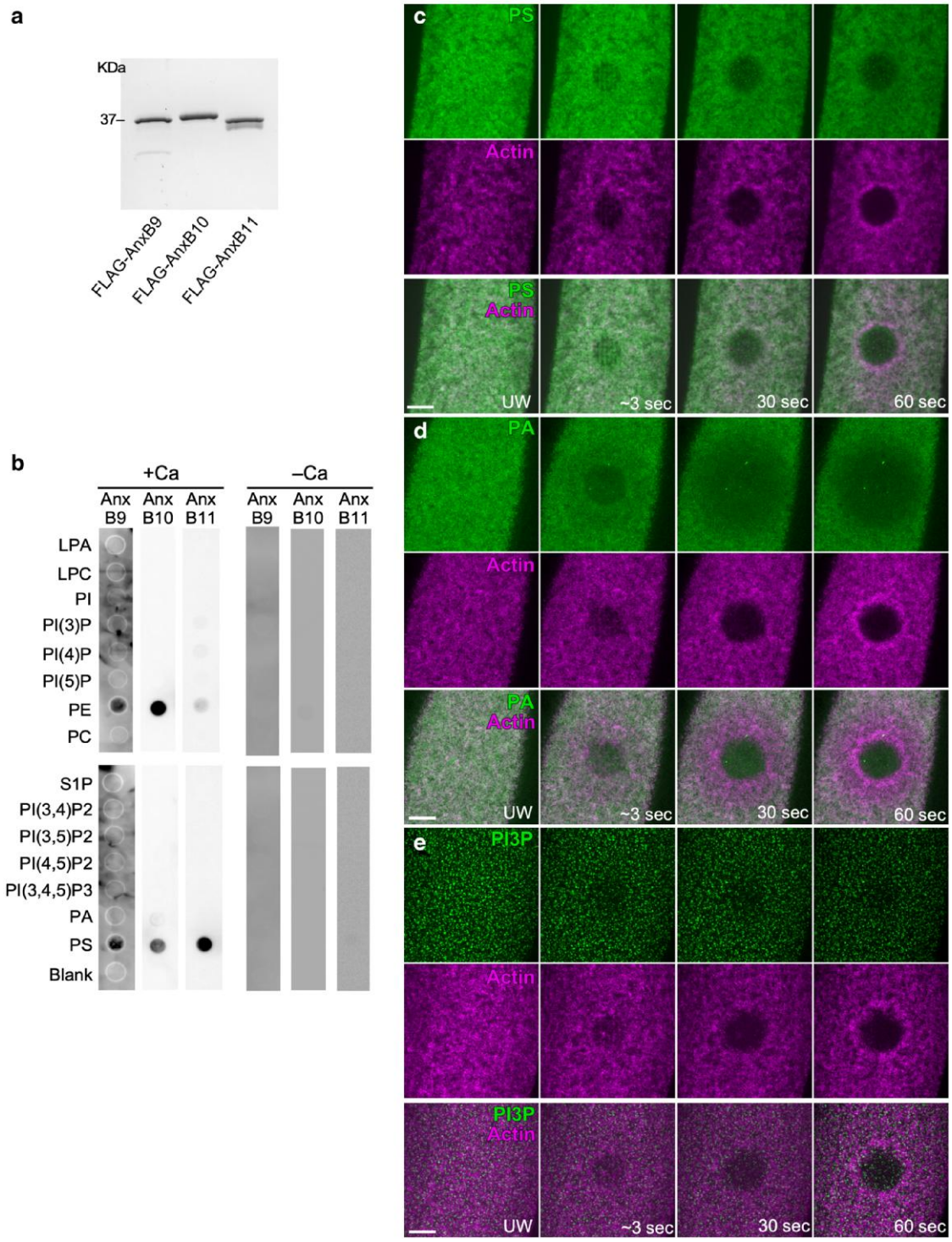

Fig. 5. Anxs do not simply respond to phospholipids during cell wound repair. a) Coomassie-stained gel showing the purified Anx proteins used in this study. b) PIP strip assays. Purified recombinant FLAG-AnxB9, FLAG-AnxB10, and FLAG-AnxB11 proteins were incubated with a PIP strip ± Ca^{2+}. (c–e) Localization of PS (c), PA (d), and PI3P (e) lipid reporters along with an actin reporter (sGMCA or sStMCA). Time after wounding is indicated. Scale bar: 20 µm.

closure (Fig. c–f; Supplementary Video 2). Thus, while cell wound repair was still initiated in embryos with reduced calcium influx, this repair was disrupted and inefficient.

Discussion

Calcium influx is one of the earliest events during cell wound repair and is one of the "start" signals that initiate the repair processes. Indeed, previous studies and this study show that cell wounds do not close in the absence of extracellular calcium influx (Bement *et al.* 1999; McNeil and Terasaki 2001; McNeil and Kirchhausen 2005; Idone *et al.* 2008; Jimenez *et al.* 2014; Talukder *et al.* 2020). Annexins are a calcium-responsive family of proteins that are recruited to cell wounds. Anxs are no longer recruited to the wound in the absence of calcium influx (Demonbreun *et al.* 2016; Koerdt and Gerke 2017; Bittel *et al.* 2020). The requirement for Anxs during

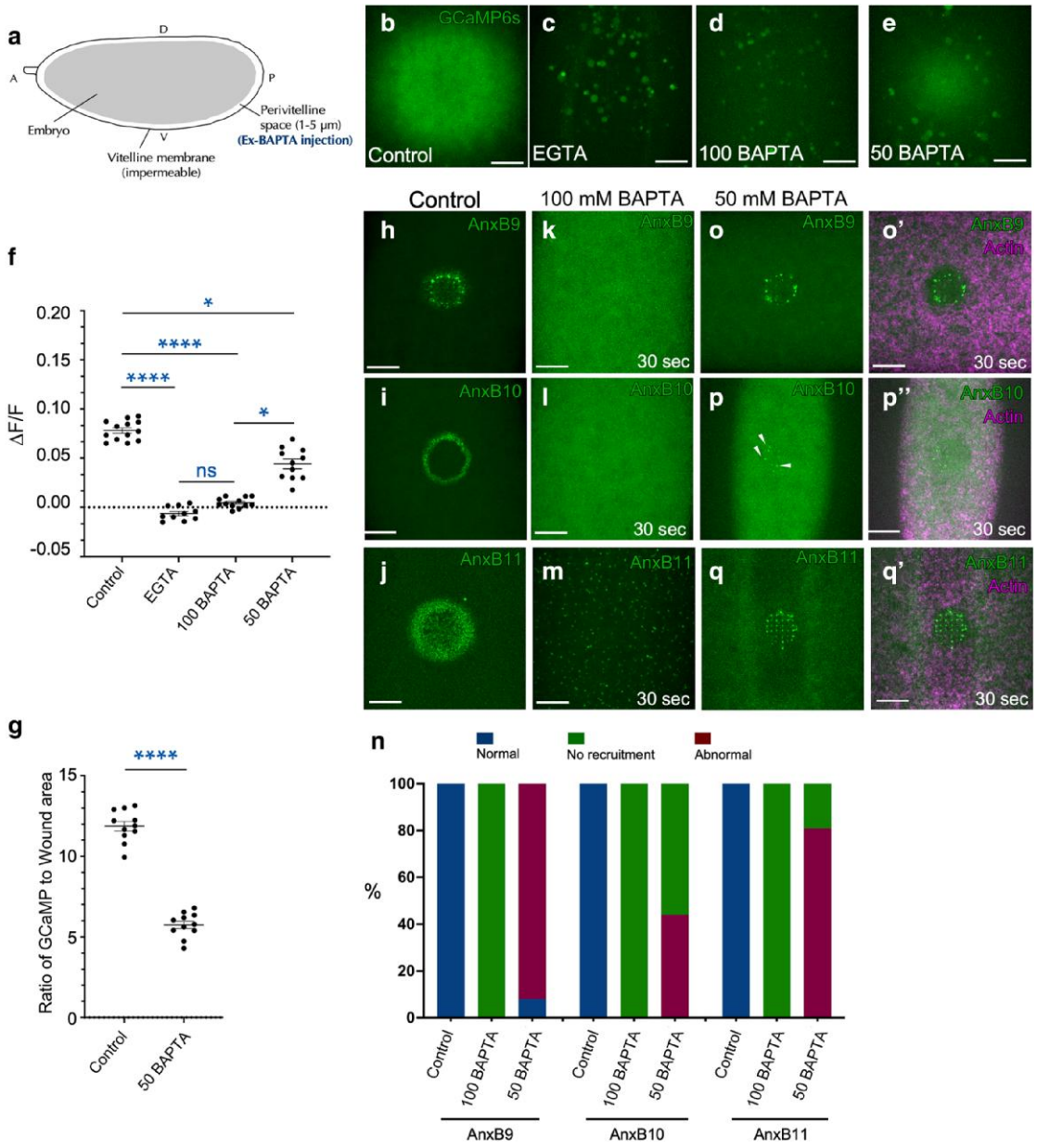

Fig. 6. Calcium dynamics regulate Anx recruitment patterns to cell wounds. a) Schemaric diagram showing the *Drosophila* embryo encapsulated by an impermeable vitelline membrane. (b–e) GCaMP signals in NC4–6 staged *Drosophila* embryos with control water injection (b), EGTA (100 mM) injection (c), BAPTA (100 mM) injection (d), or BAPTA (50 mM) injection (e). f) Quantification of GCaMP signals (ΔF/F) in the conditions of (b–e). g) Quantification of GCaMP diffusion (ratio of GCaMP area to wound area) in the conditions of (b and e). (h–m) Localization of AnxB9, AnxB10, and AnxB11 in control (h–j) or BAPTA (100 mM) injection (k–m). (n) Quantification of Anx recruitment in control and BAPTA injection. (o–q') Localization of AnxB9, AnxB10, and AnxB11 in BAPTA injection (50 mM). Time after wounding is indicated. Scale bar: 20 μm.

cell wound repair is highly conserved with different family members exhibiting different spatiotemporal recruitment patterns and functions around the wound. We find that the 3 *Drosophila* Anx proteins are recruited to cell wounds and exhibit non-identical recruitment patterns. Strikingly, we find that the level of calcium influx regulates these rapid recruitment patterns of Anxs around the wound, allowing the uniform calcium signal to generate discrete spatial patterns. The Anx patterns are required, in turn, for the distinct recruitments of RhoGEF2 and RhoGEF3 mediated by actin dynamics including actin stabilization.

While many Anxs functions involved in mammalian cell wound repair have been shown to function in membrane dynamics (Lennon *et al.* 2003; McNeil *et al.* 2006; Bouter *et al.* 2011; Bouter *et al.* 2015; Lauritzen *et al.* 2015; Carmeille *et al.* 2016; Boye *et al.* 2017; Sønder *et al.* 2019; Bittel *et al.* 2020; Croissant *et al.* 2020; 2022; Demonbreun *et al.* 2022), our previous and this study indicate that Anxs also function in actin dynamics (Nakamura *et al.* 2017). This regulation of actin dynamics is important for efficient repair through the regulation of RhoGEFs recruitment to the wound. Interestingly, we find that RhoGEF2 recruitment to the wound is regulated by the Anxs through 2 different types of actin dynamics (Fig. 8). One regulation is through actin stabilization mediated by AnxB9. The other regulation is mediated by AnxB10 and B11 that does not involve actin stabilization. In addition, while AnxB9 does not regulate RhoGEF3 recruitment, AnxB10 and AnxB11 do regulate RhoGEF3 recruitment through the stabilization of F-actin. These results suggest that the recruitment of each Anx to the distinct regions around the wound is necessary to regulate different aspects of actin dynamics required

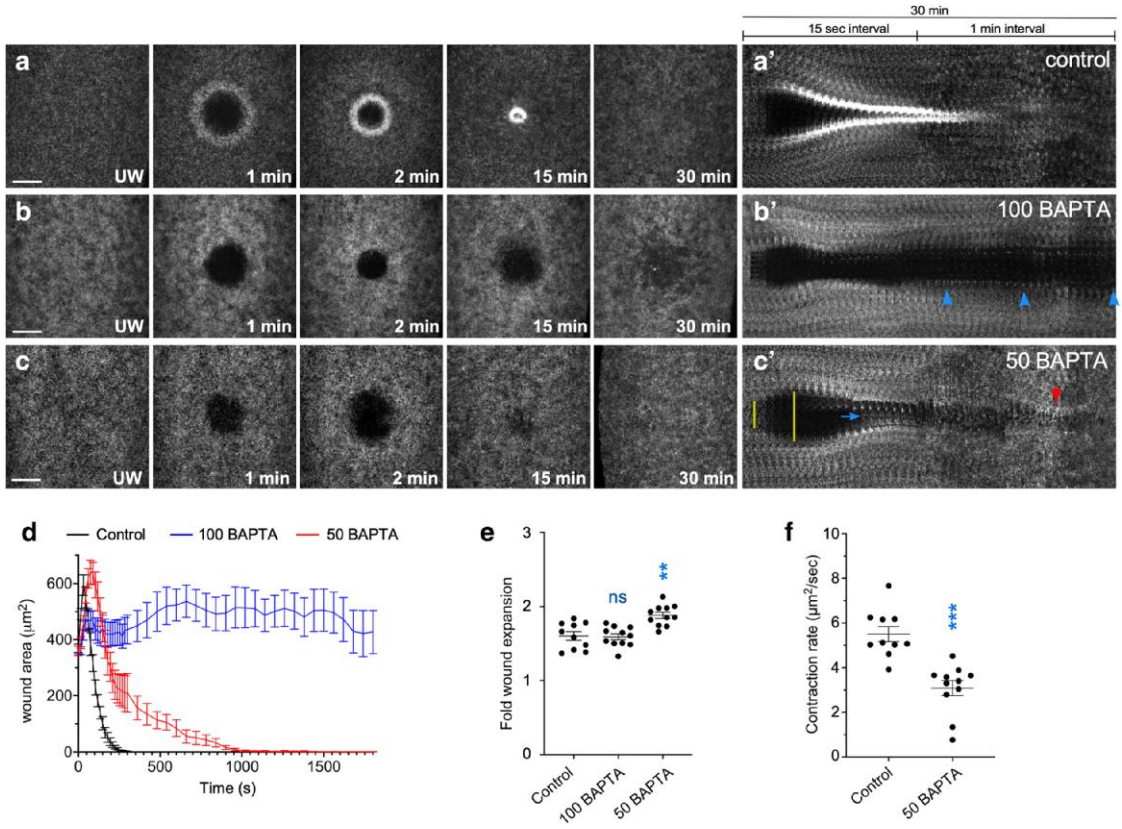

Fig. 7. Lower calcium influx impairs cell wound repair. (a–c') Actin dynamics (sGMCA) during cell wound repair in NC4–6 staged *Drosophila* embryos: control (a–a'), BAPTA (100 mM) injection (b–b'), and BAPTA (50 mM) injection (c–c'). Wound expansion is highlighted by yellow lines. Actin accumulation internal to the wound is indicated by blue arrows. Completion of wound closure is indicated by red arrowheads. Remaining the wound open is indicated by blue arrowheads. (d–f) Quantification of the wound area over time (d), fold wound expansion (e) for control ($n = 10$), BAPTA [100 mM ($n = 11$)], and BAPTA [50 mM ($n = 11$)], and contraction rate (f) for control ($n = 10$) and BAPTA [50 mM ($n = 11$)]. Error bars represent ± SEM. Scale bar: 20 µm. Time after wounding is indicated. ANOVA test was performed in *e*. Welch's *t*-test was performed in f: $^{**}P < 0.01$, ns is not significant.

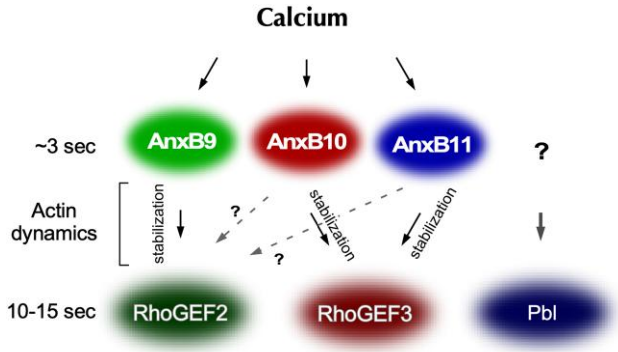

Fig. 8. Schematic diagram summarizing the calcium > Anxs > actin > RhoGEFs pathways in response to cell wounds. Anxs are rapidly recruited in a calcium-dependent manner to distinct regions around the wound to regulate actin dynamics. Subsequently, RhoGEF2 and RhoGEF3 are recruited to the wound depending on Anx-dependent actin networks, which is indispensable for the formation of robust actomyosin ring at the wound edge.

to subsequently establish the contractile actomyosin ring for wound closure. Previous studies showed that Anxs often associate with S100 family proteins to regulate actin dynamics. In mammalian cells, Annexin A2 regulates actin dynamics by associating with the S100A2 protein (Hayes *et al.* 2006; Jaiswal *et al.* 2014). No *Drosophila* homologs of S100 family proteins have been identified to date, suggesting an as-yet-unknown mechanism operates in this context.

While Anxs exhibit spatially and temporally regulated recruitment patterns around the cell wound in many different models including our *Drosophila* model, how this regulation is achieved in response to a uniform calcium influx has not been clear. Surprisingly, we find that Anxs are still recruited to the wound under conditions of reduced calcium influx, but their spatial recruitment patterns are different compared to those under normal calcium influx conditions. This suggests that calcium influx is needed to create the spatial information for precise protein recruitment around the cell wound in addition to initiating repair processes. Consistent with calcium playing multiple roles in the repair process, the amount of calcium in the media has been shown to affect cell survival rates after sonoporation, as well as actin accumulation levels at the wound (Zhou *et al.* 2008; Talukder *et al.* 2020). We find that cell wounds eventually close under conditions of reduced calcium influx, but the repair efficiency and actomyosin ring formation are highly disrupted. Downstream proteins can still be recruited around the wound, whereas their spatial misregulation prevents actin recruitment and assembly into a robust actomyosin ring.

Unexpectedly, we find that wounds do not overexpand in embryos injected with 100 mM BAPTA, suggesting that wound expansion is not regulated by simply releasing membrane tension. Indeed, while a previous study showed that reduced membrane tension is required for efficient repair (Togo *et al.* 2000), we find that Anxs regulate F-actin stabilization leading to increased membrane tension (Chugh and Paluch 2018) and their knockdowns exhibit wound overexpansion

phenotypes. Thus, wound expansion is the consequence of a balance between positive and negative regulations. Our previous study showed that many different gene knockdowns exhibit wound over-expansion phenotypes; however, embryos under conditions in which translation is inhibited exhibit less wound expansion (Nakamura *et al.* 2020). Thus, a group of proteins translated from mRNA upon wounding might have distinct functions to regulate actin and membrane dynamics for wound expansion.

Dysregulation of calcium homeostasis is associated with various diseases, including different types of cancer, muscular dystrophy, and diabetes, which also exhibit impaired cell wound repair (Levy 1999; Arruda and Hotamisligil 2015; Ahn *et al.* 2017; Monteith *et al.* 2017; Xu *et al.* 2018; Chandra *et al.* 2019; Cui *et al.* 2021). Consistent with our finding that cell wound repair is highly impaired under conditions of reduced calcium influx, intracellular calcium levels from different sources in disease conditions are known to enhance or impair cell wound repair in a context-dependent manner (Bansal *et al.* 2003; Cai *et al.* 2009; Wirtz *et al.* 2011; Cheng *et al.* 2014; Lauritzen *et al.* 2015; Quattrocelli *et al.* 2017; Chandra *et al.* 2019; Tsurumi *et al.* 2019; Bouvet *et al.* 2020; Mareedu *et al.* 2021; Ritter *et al.* 2022). For example, cancer cells have efficient cell wound repair in response to physical stresses during invasion processes (Wirtz *et al.* 2011; Bouvet *et al.* 2020; Ritter *et al.* 2022), whereas diseased cells from muscular dystrophy or diabetes backgrounds exhibit poor cell wound repair (Bansal *et al.* 2003; Cai *et al.* 2009; Cheng *et al.* 2014; Quattrocelli *et al.* 2017; Chandra *et al.* 2019; Tsurumi *et al.* 2019; Mareedu *et al.* 2021). Elucidating how a cell receives this calcium-mediated spatial information and then regulates precise protein recruitment around the wound is the next major challenge in the field.

Data availability

Strains and plasmids are available upon request. Supplementary Table 1 contains a list of flies and reagents used in this study. Supplementary Table 2 contains all quantification data for Figs. 3, 4, 6, and 7. Supplementary Video 1 contains time-lapse movies corresponding to Figs. 2 and 3. Supplementary Video 2 contains time-lapse movies corresponding to Fig. 7.

Supplemental material is available at GENETICS online.

Acknowledgments

We thank Du Guangwei, Padinjat Raghu, Tony Cooke, the Bloomington Stock Center (National Institutes of Health P40OD018537), the Kyoto Stock Center, the Harvard Transgenic RNAi Project (Office of the Director R24 OD030002), FlyBase (FB2024_03), the Fred Hutch/Leica Center of Excellence, and the Drosophila Genome Resource Center (National Institutes of Health 2P40OD010949) for advice, microscopes, antibodies, DNAs, flies, and other reagents used in this study.

Funding

This research was supported by National Institutes of Health GM111635, the Mark Groudine Chair for Outstanding Achievements in Science and Service (to SMP), and the National Cancer Institute Cancer Center Support Grant P30 CA015704 (for Shared Resources).

Conflicts of interest

The author(s) declare no conflict of interest.

Author contributions

MN and SMP designed the experiments and analyzed the resulting data. MN performed the experiments. MN and SMP wrote the manuscript.

Literature cited

Abreu-Blanco MT, Verboon JM, Parkhurst SM. 2011. Cell wound repair in *Drosophila* occurs through three distinct phases of membrane and cytoskeletal remodeling. J Cell Biol. 193(3):455–464. doi:10.1083/jcb.201011018.

Ahn C, Kang JH, Jeung EB. 2017. Calcium homeostasis in diabetes mellitus. J Vet Sci. 18(3):261–266. doi:10.4142/jvs.2017.18.3.261.

Andrews NW, Corrotte M. 2018. Plasma membrane repair. Curr Biol. 28(8):R392–R397. doi:10.1016/j.cub.2017.12.034.

Arruda AP, Hotamisligil GS. 2015. Calcium homeostasis and organelle function in the pathogenesis of obesity and diabetes. Cell Metab. 22(3):381–397. doi:10.1016/j.cmet.2015.06.010.

Ashraf APK, Gerke V. 2021. Plasma membrane wound repair is characterized by extensive membrane lipid and protein rearrangements in vascular endothelial cells. Biochim Biophys Acta. 1868(7):118991. doi:10.1016/j.bbamcr.2021.118991.

Babbin BA, Parkos CA, Mandell KJ, Winfree LM, Laur O, Ivanov AI, Nusrat A. 2007. Annexin 2 regulates intestinal epithelial cell spreading and wound closure through Rho-related signaling. Am J Pathol. 170(3):951–966. doi:10.2353/ajpath.2007.060647.

Bansal D, Miyake K, Vogel SS, Groh S, Chen CC, Williamson R, McNeil PL, Campbell KP. 2003. Defective membrane repair in dysferlin-deficient muscular dystrophy. Nature. 423(6936):168–172. doi:10.1038/nature01573.

Bement WM, Mandato CA, Kirsch MN. 1999. Wound-induced assembly and closure of an actomyosin purse string in Xenopus oocytes. Curr Biol. 9(11):579–587. doi:10.1016/S0960-9822(99)80261-9.

Benaud C, Le Dez G, Mironov S, Galli F, Reboutier D, Prigent C. 2015. Annexin A2 is required for the early steps of cytokinesis. EMBO Rep. 16(4):481–489. doi:10.15252/embr.201440015.

Benaud C, Prigent C. 2016. Annexin A2: a new player in mitosis. Cell cycle. 15(1):9–10. doi:10.1080/15384101.2015.1115643.

Bittel DC, Chandra G, Tirunagri LMS, Deora AB, Medikayala S, Scheffer L, Defour A, Jaiswal JK. 2020. Annexin A2 mediates dysferlin accumulation and muscle cell membrane repair. Cells. 9(9):1919. doi:10.3390/cells9091919.

Blackwood RA, Ernst JD. 1990. Characterization of Ca2(+)-dependent phospholipid binding, vesicle aggregation and membrane fusion by Annexins. Biochem J. 266(1):195–200. doi:10.1042/bj2660195.

Bouter A, Carmeille R, Gounou C, Bouvet F, Degrelle SA, Evain-Brion D, Brisson AR. 2015. Review: Annexin-A5 and cell membrane repair. Placenta. 36(Suppl. 1):S43–S49. doi:10.1016/j.placenta.2015.01.193.

Bouter A, Gounou C, Berat R, Tan S, Gallois B, Granier T, d'Estaintot BL, Poschl E, Brachvogel B, Brisson AR. 2011. Annexin-A5 assembled into two-dimensional arrays promotes cell membrane repair. Nat Commun. 2(1):270. doi:10.1038/ncomms1270.

Bouvet F, Ros M, Bonedeau E, Croissant C, Frelin L, Saltel F, Moreau V, Bouter A. 2020. Defective membrane repair machinery impairs survival of invasive cancer cells. Sci Rep. 10(1):21821. doi:10.1038/s41598-020-77902-5.

Boye TL, Maeda K, Pezeshkian W, Sønder SL, Haeger SC, Gerke V, Simonsen AC, Nylandsted J. 2017. Annexin A4 and A6 induce membrane curvature and constriction during cell membrane repair. Nat Commun. 8(1):1623. doi:10.1038/s41467-017-01743-6.

Brand AH, Perrimon N. 1993. Targeted gene expression as a means of altering cell fates and generating dominant phenotypes. Development. 118(2):401–415. doi:10.1242/dev.118.2.401.

Cai C, Weisleder N, Ko JK, Komazaki S, Sunada Y, Nishi M, Takeshima H, Ma J. 2009. Membrane repair defects in muscular dystrophy are linked to altered interaction between MG53, caveolin-3, and dysferlin. J Biol Chem. 284(23):15894–15902. doi:10.1074/jbc.M109.009589.

Carmeille R, Bouvet F, Tan S, Croissant C, Gounou C, Mamchaoui K, Mouly V, Brisson AR, Bouter A. 2016. Membrane repair of human skeletal muscle cells requires Annexin-A5. Biochim Biophys Acta. 1863(9):2267–2279. doi:10.1016/j.bbamcr.2016.06.003.

Chandra G, Defour A, Mamchoui K, Pandey K, Mishra S, Mouly V, Sreetama S, Mahad Ahmad M, Mahjneh I, Morizono H, *et al.* 2019. Dysregulated calcium homeostasis prevents plasma membrane repair in Anoctamin 5/TMEM16E-deficient patient muscle cells. Cell Death Discov. 5(1):118. doi:10.1038/s41420-019-0197-z.

Cheng X, Zhang X, Gao Q, Ali Samie M, Azar M, Tsang WL, Dong L, Sahoo N, Li X, Zhuo Y, *et al.* 2014. The intracellular Ca^{2+} channel MCOLN1 is required for sarcolemma repair to prevent muscular dystrophy. Nat Med. 20(10):1187–1192. doi:10.1038/nm.3611.

Cheng X, Zhang X, Yu L, Xu H. 2015. Calcium signaling in membrane repair. Semin Cell Dev Biol. 45:24–31. doi:10.1016/j.semcdb.2015.10.031.

Chugh P, Paluch EK. 2018. The actin cortex at a glance. J Cell Sci. 131(14):jcs186254. doi:10.1242/jcs.186254.

Cooper ST, McNeil PL. 2015. Membrane repair: mechanisms and pathophysiology. Physiol Rev. 95(4):1205–1240. doi:10.1152/physrev.00037.2014.

Croissant C, Gounou C, Bouvet F, Tan S, Bouter A. 2020. Annexin-A6 in membrane repair of human skeletal muscle cell: a role in the cap subdomain. Cells. 9(7):1742. doi:10.3390/cells9071742.

Croissant C, Gounou C, Bouvet F, Tan S, Bouter A. 2022. Trafficking of Annexins during membrane repair in human skeletal muscle cells. Membranes. 12(2):153. doi:10.3390/membranes12020153.

Cui C, Zhang Y, Liu G, Zhang S, Zhang J, Wang X. 2021. Advances in the study of cancer metastasis and calcium signaling as potential therapeutic targets. Explor Target Antitumor Ther. 2(3):266–291. doi:10.37349/etat.2021.00046.

Davenport NR, Sonnemann KJ, Eliceiri KW, Bement WM. 2016. Membrane dynamics during cellular wound repair. Mol Biol Cell. 27(14):2272–2285. doi:10.1091/mbc.E16-04-0223.

Demonbreun AR, Bogdanovic E, Vaught LA, Reiser NL, Fallon KS, Long AM, Oosterbaan CC, Hadhazy M, Page PGT, Joseph PRB, *et al.* 2022. A conserved annexin A6–mediated membrane repair mechanism in muscle, heart, and nerve. JCI Insight. 7(14):e158107. doi:10.1172/jci.insight.158107.

Demonbreun AR, Quattrocelli M, Barefield DY, Allen MV, Swanson KE, McNally EM. 2016. An actin-dependent annexin complex mediates plasma membrane repair in muscle. J Cell Biol. 213(6):705–718. doi:10.1083/jcb.201512022.

Ebstrup ML, Dias C, Heitmann ASB, Sønder SL, Nylandsted J. 2021. Actin cytoskeletal dynamics in single-cell wound repair. Int J Mol Sci. 22(19):10886. doi:10.3390/ijms221910886.

Eisenberg S, Haimov E, Walpole GFW, Plumb J, Kozlov MM, Grinstein S. 2021. Mapping the electrostatic profiles of cellular membranes. Mol Biol Cell. 32(3):301–310. doi:10.1091/mbc.E19-08-0436.

Gabel M, Delavoie F, Demais V, Royer C, Bailly Y, Vitale N, Bader MF, Chasserot-Golaz S. 2015. Annexin A2-dependent actin bundling promotes secretory granule docking to the plasma membrane and exocytosis. J Cell Biol. 210(5):785–800. doi:10.1083/jcb.201412030.

Gerke V, Creutz CE, Moss SE. 2005. Annexins: linking Ca^{2+} signalling to membrane dynamics. Nat Rev Mol Cell Biol. 6(6):449–461. doi:10.1038/nrm1661.

Glenney JR Jr., Tack B, Powell MA. 1987. Calpactins: two distinct Ca^{++}-regulated phospholipid- and actin-binding proteins isolated from lung and placenta. J Cell Biol. 104(3):503–511. doi:10.1083/jcb.104.3.503.

Hayes MJ, Rescher U, Gerke V, Moss SE. 2004. Annexin-actin interactions. Traffic. 5(8):571–576. doi:10.1111/j.1600-0854.2004.00210.x.

Hayes MJ, Shao D, Bailly M, Moss SE. 2006. Regulation of actin dynamics by annexin 2. EMBO J. 25(9):1816–1826. doi:10.1038/sj.emboj.7601078.

Hosoya H, Kobayashi R, Tsukita S, Matsumura F. 1992. Ca^{2+}-regulated actin and phospholipid binding protein (68 kD-protein) from bovine liver: identification as a homologue for annexin VI and intracellular localization. Cell Motil Cytoskeleton. 22(3):200–210. doi:10.1002/cm.970220307.

Hui J, Nakamura M, Dubrulle J, Parkhurst SM. 2023. Coordinated efforts of different actin filament populations are needed for optimal cell wound repair. Mol Biol Cell. 34(3):ar15. doi:10.1091/mbc.E22-05-0155.

Hui J, Stjepić V, Nakamura M, Parkhurst SM. 2022. Wrangling actin assemblies: actin ring dynamics during cell wound repair. Cells. 11(18):2777. doi:10.3390/cells11182777.

Idone V, Tam C, Goss JW, Toomre D, Pypaert M, Andrews NW. 2008. Repair of injured plasma membrane by rapid Ca^{2+}-dependent endocytosis. J Cell Biol. 180(5):905–914. doi:10.1083/jcb.200708010.

Ikebuchi NW, Waisman DM. 1990. Calcium-dependent regulation of actin filament bundling by lipocortin-85. J Biol Chem. 265(6):3392–3400. doi:10.1016/S0021-9258(19)39780-7.

Jaiswal JK, Lauritzen SP, Scheffer L, Sakaguchi M, Bunkenborg J, Simon SM, Kallunki T, Jäättelä M, Nylandsted J. 2014. S100a11 is required for efficient plasma membrane repair and survival of invasive cancer cells. Nat Commun. 5(1):3795. doi:10.1038/ncomms4795.

Jimenez AJ, Maiuri P, Lafaurie-Janvore J, Divoux S, Piel M, Perez F. 2014. ESCRT machinery is required for plasma membrane repair. Science. 343(6174):1247136. doi:10.1126/science.1247136.

Kiehart DP, Galbraith CG, Edwards KA, Rickoll WL, Montague RA. 2000. Multiple forces contribute to cell sheet morphogenesis for dorsal closure in *Drosophila*. J Cell Biol. 149(2):471–490. doi:10.1083/jcb.149.2.471.

Koerdt SN, Gerke V. 2017. Annexin A2 is involved in Ca(2+)-dependent plasma membrane repair in primary human endothelial cells. Biochim Biophys Acta. 1864(6):1046–1053. doi:10.1016/j.bbamcr.2016.12.007.

Lauritzen SP, Boye TL, Nylandsted J. 2015. Annexins are instrumental for efficient plasma membrane repair in cancer cells. Semin Cell Dev Biol. 45:32–38. doi:10.1016/j.semcdb.2015.10.028.

Lee PT, Zirin J, Kanca O, Lin WW, Schulze KL, Li-Kroeger D, Tao R, Devereaux C, Hu Y, Chung V, *et al.* 2018. A gene-specific T2A-GAL4 library for *Drosophila*. Elife. 7:e35574. doi:10.7554/eLife.35574.

Lennon NJ, Kho A, Bacskai BJ, Perlmutter SL, Hyman BT, Brown RH. 2003. Dysferlin interacts with Annexins A1 and A2 and mediates sarcolemmal wound-healing. J Biol Chem. 278(50):50466–50473. doi:10.1074/jbc.M307247200.

Levy J. 1999. Abnormal cell calcium homeostasis in type 2 diabetes mellitus: a new look on old disease. Endocrine. 10(1):1–6. doi:10.1385/ENDO:10:1:1.

Liu R, Abreu-Blanco MT, Barry KC, Linardopoulou EV, Osborn GE, Parkhurst SM. 2009. Wash functions downstream of Rho and links linear and branched actin nucleation factors. Development. 136(16):2849–2860. doi:10.1242/dev.035246.

Lizarbe M, Barrasa J, Olmo N, Gavilanes F, Turnay J. 2013. Annexin-phospholipid interactions. Functional implications. Int J Mol Sci. 14(2):2652–2683. doi:10.3390/ijms14022652.

Mareedu S, Million ED, Duan D, Babu GJ. 2021. Abnormal calcium handling in Duchenne muscular dystrophy: mechanisms and potential therapies. Front Physiol. 12:647010. doi:10.3389/fphys.2021.647010.

McNeil AK, Rescher U, Gerke V, McNeil PL. 2006. Requirement for Annexin A1 in plasma membrane repair. J Biol Chem. 281(46):35202–35207. doi:10.1074/jbc.M606406200.

McNeil PL, Kirchhausen T. 2005. An emergency response team for membrane repair. Nat Rev Mol Cell Biol. 6(6):499–505. doi:10.1038/nrm1665.

McNeil PL, Terasaki M. 2001. Coping with the inevitable: how cells repair a torn surface membrane. Nat Cell Biol. 3(5):E124–E129. doi:10.1038/35074652.

Moe A, Golding AE, Bement WM. 2015. Cell healing: calcium, repair and regeneration. Semin Cell Dev Biol. 45:18–23. doi:10.1016/j.semcdb.2015.09.026.

Monteith GR, Prevarskaya N, Roberts-Thomson SJ. 2017. The calcium–cancer signalling nexus. Nat Rev Cancer. 17(6):373–380. doi:10.1038/nrc.2017.18.

Morel E, Parton RG, Gruenberg J. 2009. Annexin A2-dependent polymerization of actin mediates endosome biogenesis. Dev Cell. 16(3):445–457. doi:10.1016/j.devcel.2009.01.007.

Nakamura M, Dominguez ANM, Decker JR, Hull AJ, Verboon JM, Parkhurst SM. 2018. Into the breach: how cells cope with wounds. Open Biol. 8(10):180135. doi:10.1098/rsob.180135.

Nakamura M, Verboon JM, Allen TE, Abreu-Blanco MT, Liu R, Dominguez ANM, Delrow JJ, Parkhurst SM. 2020. Autocrine insulin pathway signaling regulates actin dynamics in cell wound repair. PLoS Genet. 16(12):e1009186. doi:10.1371/journal.pgen.1009186.

Nakamura M, Verboon JM, Parkhurst SM. 2017. Prepatterning by RhoGEFs governs Rho GTPase spatiotemporal dynamics during wound repair. J Cell Biol. 216(12):3959–3969. doi:10.1083/jcb.201704145.

Ni J-Q, Zhou R, Czech B, Liu L-P, Holderbaum L, Yang-Zhou D, Shim H-S, Tao R, Handler D, Karpowicz P, *et al.* 2011. A genome-scale shRNA resource for transgenic RNAi in *Drosophila*. Nat Methods. 8(5):405–407. doi:10.1038/nmeth.1592.

Öztürk-Çolak A, Marygold SJ, Antonazzo G, Attrill H, Goutte-Gattat D, Jenkins VK, Matthews BB, Millburn G, Dos Santos G, Tabone CJ, *et al.* 2024. FlyBase: updates to the *Drosophila* genes and genomes database. Genetics. 227(1):iyad211. doi:10.1093/genetics/iyad211.

Pervin MS, Itoh G, Talukder MSU, Fujimoto K, Morimoto YV, Tanaka M, Ueda M, Yumura S. 2018. A study of wound repair in Dictyostelium cells by using novel laserporation. Sci Rep. 8(1):7969. doi:10.1038/s41598-018-26337-0.

Quattrocelli M, Capote J, Ohiri JC, Warner JL, Vo AH, Earley JU, Hadhazy M, Demonbreun AR, Spencer MJ, McNally EM. 2017. Genetic modifiers of muscular dystrophy act on sarcolemmal resealing and recovery from injury. PLoS Genet. 13(10):e1007070. doi:10.1371/journal.pgen.1007070.

Rescher U, Ludwig C, Konietzko V, Kharitonenkov A, Gerke V. 2008. Tyrosine phosphorylation of Annexin A2 regulates Rho-mediated actin rearrangement and cell adhesion. J Cell Sci. 121(13):2177–2185. doi:10.1242/jcs.028415.

Ritter AT, Shtengel G, Xu CS, Weigel A, Hoffman DP, Freeman M, Iyer N, Alivodej N, Ackerman D, Voskoboinik I, *et al.* 2022. ESCRT-mediated membrane repair protects tumor-derived cells against T cell attack. Science. 376(6591):377–382. doi:10.1126/science.abl3855.

Schindelin J, Arganda-Carreras I, Frise E, Kaynig V, Longair M, Pietzsch T, Preibisch S, Rueden C, Saalfeld S, Schmid B, *et al.* 2012. Fiji: an open-source platform for biological-image analysis. Nat Methods. 9(7):676–682. doi:10.1038/nmeth.2019.

Sønder SL, Boye TL, Tölle R, Dengjel J, Maeda K, Jäättelä M, Simonsen AC, Jaiswal JK, Nylandsted J. 2019. Annexin A7 is required for ESCRT III-mediated plasma membrane repair. Sci Rep. 9(1):6726. doi:10.1038/s41598-019-43143-4.

Sonnemann KJ, Bement WM. 2011. Wound repair: toward understanding and integration of single-cell and multicellular wound responses. Annu Rev Cell Dev Biol. 27(1):237–263. doi:10.1146/annurev-cellbio-092910-154251.

Spradling AC. 1986. P element-mediated transformation. In: Roberts DB, editors. Drosophila: A Practical Approach. Oxford: IRL Press. p. 175–197.

Talukder MSU, Pervin MS, Tanvir MIO, Fujimoto K, Tanaka M, Itoh G, Yumura S. 2020. Ca^{2+}-calmodulin dependent wound repair in Dictyostelium cell membrane. Cells. 9(4):1058. doi:10.3390/cells9041058.

Terasaki M, Miyake K, McNeil PL. 1997. Large plasma membrane disruptions are rapidly resealed by Ca^{2+}-dependent vesicle-vesicle fusion events. J Cell Biol. 139(1):63–74. doi:10.1083/jcb.139.1.63.

Thakur R, Naik A, Panda A, Raghu P. 2019. Regulation of membrane turnover by phosphatidic acid: cellular functions and disease implications. Front Cell Dev Biol. 7:83. doi:10.3389/fcell.2019.00083.

Togo T, Krasieva TB, Steinhardt RA. 2000. A decrease in membrane tension precedes successful cell-membrane repair. Mol Biol Cell. 11(12):4339–4346. doi:10.1091/mbc.11.12.4339.

Tsurumi F, Baba S, Yoshinaga D, Umeda K, Hirata T, Takita J, Heike T. 2019. The intracellular Ca^{2+} concentration is elevated in cardiomyocytes differentiated from hiPSCs derived from a Duchenne muscular dystrophy patient. PLoS One. 14(3):e0213768. doi:10.1371/journal.pone.0213768.

Vaughan EM, You JS, Elsie Yu HY, Lasek A, Vitale N, Hornberger TA, Bement WM. 2014. Lipid domain-dependent regulation of single-cell wound repair. Mol Biol Cell. 25(12):1867–1876. doi:10.1091/mbc.e14-03-0839.

Vicic N, Guo X, Chan D, Flanagan JG, Sigal IA, Sivak JM. 2022. Evidence of an Annexin a4 mediated plasma membrane repair response to biomechanical strain associated with glaucoma pathogenesis. J Cell Physiol. 237(9):3687–3702. doi:10.1002/jcp.30834.

Wirtz D, Konstantopoulos K, Searson PC. 2011. The physics of cancer: the role of physical interactions and mechanical forces in metastasis. Nat Rev Cancer. 11(7):512–522. doi:10.1038/nrc3080.

Xu M, Seas A, Kiyani M, Ji KSY, Bell HN. 2018. A temporal examination of calcium signaling in cancer- from tumorigenesis, to immune evasion, and metastasis. Cell Biosci. 8(1):25. doi:10.1186/s13578-018-0223-5.

Yeung T, Gilbert GE, Shi J, Silvius J, Kapus A, Grinstein S. 2008. Membrane phosphatidylserine regulates surface charge and protein localization. Science. 319(5860):210–213. doi:10.1126/science.1152066.

Zhang F, Wang Z, Lu M, Yonekubo Y, Liang X, Zhang Y, Wu P, Zhou Y, Grinstein S, Hancock JF, *et al.* 2014. Temporal production of the signaling lipid phosphatidic acid by phospholipase D2 determines the output of extracellular signal-regulated kinase signaling in cancer cells. Mol Cell Biol. 34(1):84–95. doi:10.1128/MCB.00987-13.

Zhou Y, Shi J, Cui J, Deng CX. 2008. Effects of extracellular calcium on cell membrane resealing in sonoporation. J Control Release. 126(1):34–43. doi:10.1016/j.jconrel.2007.11.007.

Editor: D. Andrew